Serb. Astron. J. № 191 (2015), 29 - 37 **UDC 524.354–77**
DOI: 10.2298/SAJ150715004O Original scientific paper

ON THE INTEGRATED CONTINUUM RADIO SPECTRUM OF SUPERNOVA REMNANT W44 (G34.7-0.4): NEW INSIGHTS FROM PLANCK

D. Onić

Department of Astronomy, Faculty of Mathematics, University of Belgrade
Studentski trg 16, 11000 Belgrade, Serbia

E–mail: *donic@math.rs*

(Received: July 15, 2015; Accepted: October 2, 2015)

SUMMARY: In this paper, the integrated continuum radio spectrum of supernova remnant (SNR) W44 was analyzed up to 70 GHz by testing different emission models that can be responsible for its particular shape. The observations by the *Planck* space telescope made it possible to analyze the high frequency part of radio emission from SNRs. Although the quality of radio continuum spectrum (a high scatter of data points at same frequencies) prevents us to make definite conclusions, the possibility of spinning the dust emission detection towards this remnant is emphasized. In addition, a concave-down feature due to synchrotron losses can not be definitely dismissed by the present knowledge of the integrated radio continuum spectrum of this SNR.

Key words. ISM: individual (W44) – ISM: supernova remnants – radio continuum: ISM

1. INTRODUCTION

Supernova remnant W44 (G34.7-0.4, 3C392) represents one of the most interesting SNRs. It is a member of the mixed-morphology (thermal composite) class of SNRs characterized by a bright non-thermal shell-like radio morphology and centrally concentrated thermal X-ray emission (Rho and Petre 1998, Vink 2012). W44 is a middle-aged SNR (possibly around 20 000 yrs old) that has an asymmetric, quasi-elliptical, shell morphology presumably due to expansion in an inhomogeneous interstellar medium (Cardillo et al. 2014). It is about half a degree in size ($35' \times 27'$) at a distance of around 3 kpc, and it is located in a complex region of the inner Galactic plane rich in both thermal and non-thermal sources (Castelletti et al. 2007). In fact, this remnant is well placed in the W48 molecular cloud complex, a rich star-forming region.

SNR W44 constitutes one of the few demonstrated cases of an SNR-molecular cloud interacting system (Castelletti et al. 2007, and references therein). It is also detected in γ-rays. Cardillo et al. (2014) concluded that the γ-ray emission is most probably caused by the neutral pion decay (hadronic scenario). They also determined that the average gas density of regions emitting 100 MeV - 10 GeV γ-rays is relatively high ($250 - 300$ cm^{-3}). Yoshiike et al. (2013) confirmed that the W44 SNR environment consists of both molecular and atomic hydrogen and they concluded that molecular clouds, which are likely associated with this remnant, surround the radio shell. Their analysis also supports a hadronic origin of the γ-rays.

The global integrated radio continuum spectral index of this SNR is $\alpha = 0.37$ (Green 2014), where the spectral index is defined as $S_\nu \propto \nu^{-\alpha}$ with S_ν being the flux density. This is significantly less than 0.5, the value predicted by the test-particle diffusive shock acceleration theory (DSA, Urošević 2014, and references therein). On the other hand, such spectral index values are common for majority of mixed-morphology SNRs (Onić 2013, and references therein). Uchida et al. (2012) reported another common feature for mixed-morphology SNRs: radiative recombination continua of highly ionized atoms in the X-ray spectrum. They concluded that the spectrum is well reproduced by a thermal plasma in a recombining phase.

The spatially resolved radio spectral index study revealed that the detected localized absorption has a negligible influence on the total integrated flux, and thus has no measurable impact on the integrated continuum spectrum (Castelletti et al. 2007). The most likely explanation of the particular local spectral inversion is the low-frequency radio continuum free-free absorption from the ionized gas in the post shock region at the SNR/molecular cloud interface. An alternative explanation is that the thermal absorption is occurring inside the boundaries of the coincident H II region, along its periphery where the thermal electron density might be the highest. The spectral inversion is probably produced by a combination of both these effects (Castelletti et al. 2007).

It is worth mentioning that there is no evidence in the radio continuum spectrum of any coupling between the associated pulsar PSR B1853+01 and the surrounding SNR shell that could, for example, be observed as a gradual steepening from the pulsar to the shell (Castelletti et al. 2007). In addition, the pulsar wind powers a small synchrotron nebula observed at radio frequencies and X-rays (Anderl et al. 2014 and references therein).

A very interesting discovery of hard X-ray emission from the SNR, not connected with associated pulsar or correspondent pulsar wind nebula, was reported by Uchida et al. (2012). They found that hard X-rays have an arc-like structure spatially-correlated with a radio continuum filament. Uchida et al. (2012) noted that the surface brightness distribution shows a clear anti-correlation with ^{12}CO($J = 2-1$) emission from a molecular cloud. Finally, they concluded that the hard X-rays are most likely due to a synchrotron enhancement in the vicinity of the cloud. In fact, the localized non-thermal X-ray emission, as seen in the case of W44, probably reflects the physics of shock propagation in a clumpy medium. In an inter-clump gas with a lower density, cloud shocks can propagate much faster than in the dense clumps, so they can possibly accelerate high-energy electrons capable to emit X-rays (Lee et al. 2015).

Using *Spitzer* mid-IR observations, an H II region located just outside the southeastern limb of SNR W44, was detected by Castelletti et al. (2007). They showed that the combination of 8 and 24 μm *Spitzer* images reveals the hot dust grains in the Strömgren sphere, limited to the east by an annular photo dissociation region (PDR) dominated by polycyclic aromatic hydrocarbons (PAHs) emitting near 8 μm. Castelletti et al. (2007) noted that exactly at the interface between observed H II region and W44, as seen in the plane of the sky, a young stellar object is present. In fact, two massive young stellar objects are identified at the border of the H II region that is evolving within a molecular cloud shocked by the SNR W44 (Paron et al. 2009, Ortega et al. 2010).

Recently, the observations from a microwave survey of Galactic SNRs made by *Planck*[1] were published (Planck Collaboration Int. XXXI 2014). *Planck* observed the sky in nine frequency bands covering 30 - 857 GHz with high sensitivity and a range of angular resolutions from $31'$ to $5'$ (Planck Collaboration Int. XXXI 2014 and references therein). The Low Frequency Instrument covers the 30, 44, and 70 GHz bands while the High Frequency Instrument covers the 100, 143, 217, 353, 545, and 857 GHz bands.

Planck Collaboration Int. XXXI (2014) reported that the synchrotron emission from SNR W44 is detected at levels above the emission from nearby unrelated regions at 30-70 GHz. They also noted that the measured 70 GHz flux density from *Planck* is somewhat lower than that expected from the radio power law while the 30 GHz flux density is higher. Planck Collaboration Int. XXXI (2014), on the other hand, discounted the 30 GHz flux density due to possible confusion with unrelated large-scale emission from the Galactic plane. Also, it must be noted that the *Planck's* flux density measurements above 100 GHz are contaminated by an unrelated foreground emission. Planck Collaboration Int. XXXI (2014) identified a particular structure at the eastern border of the radio SNR as a compact H II region unrelated to the W44 SNR but possibly a member of the same OB association as the progenitor.

In this paper, we have analyzed the radio spectrum of the W44 SNR up to 70 GHz by testing different emission models to replicate its particular spectral shape.

2. ANALYSIS AND RESULTS

Flux densities at different frequencies for the SNR W44 were taken from Table 2 by Castelletti et al. (2007), Table 1 of Sun et al. (2011) and Table 3 of Planck Collaboration Int. XXXI (2014) in the frequency range from 610 MHz to 70 GHz. Only flux densities with errors $< 20\%$ were used in the analysis and only data corrected to the scale of Baars et al. (1977) are taken from Castelletti et al. (2007). Finally, the misprint in Table 2 of Castelletti et al.

[1] *Planck* is a project of the European Space Agency (ESA) with instruments provided by two scientific consortia funded by ESA member states, with contributions from NASA (USA) and telescope reflectors provided by a collaboration between ESA and a scientific consortium led and funded by Denmark.

(2007) regarding the data uncertainties taken from Altenhoff et al. (1970) is taken into account - uncertainties are set to 10% of the selected flux densities.

The significant scatter of flux densities measured at the same frequencies makes the integrated continuum radio spectrum difficult to analyze (see Fig. 6 by Castelletti et al. 2007 and Figures in this paper). The data come from a wide variety of telescopes with different beam sizes, which can have a significant impact on flux density measurements since W44 lies within a particularly complex region close to the Galactic plane. The effects of possible contamination by the unrelated sources can be sufficiently significant to account for the scatter in the radio continuum spectrum of W44.

2.1. The synchrotron emission from the SNR W44

The usual interpretation of the radio continuum spectrum of SNRs is that of a simple power law that arises from the synchrotron emission of charges accelerated by a diffusive shock acceleration (DSA) mechanism (Urošević 2014, and references therein). In this case, the flux density is given by the following relation (Eq. 1):

$$S_{[\mathrm{Jy}]}(\nu) = S_{[\mathrm{Jy}]}(1\mathrm{GHz})\ \nu_{[\mathrm{GHz}]}^{-\alpha}, \qquad (1)$$

where α is the radio spectral index. On the other hand, the high frequency part of the W44 radio spectrum clearly indicates that this simple model does not explain adequately the integrated continuum of this SNR. The lower value of the flux density at 70 GHz could be a possible indication of high frequency spectral bending (Planck Collaboration Int. XXXI 2014) that can be represented by (Eq. 2):

$$S_{[\mathrm{Jy}]}(\nu) = S_{[\mathrm{Jy}]}(1\mathrm{GHz})\ \nu_{[\mathrm{GHz}]}^{-\alpha}\ e^{-\frac{\nu}{\nu_0}}, \qquad (2)$$

where ν_0 is the characteristic cut-off frequency.

We performed the least-squares fits to the radio spectrum (Fig. 1) using a simple synchrotron model (solid line) as well as a synchrotron model with exponential cutoff (dotted line). The thick and thin lines in Fig. 1 correspond to fits without and with the inclusion of the *Planck* 30 GHz flux density, respectively. *Planck* data is represented by a diamond symbol except for the data point at 30 GHz which is labeled by a triangle. The best fitting parameters for these two models are presented in Table 1. The asterisk symbol in Table 1 indicates where *Planck* data at 30 GHz is included in the fit.

It is known that the radio spectra of evolved SNRs could appear in a concave-down form. This kind of spectrum can be explained using the DSA theory with the effect of synchrotron losses within the finite emission region. Generally, the concave-down form of the radio spectra should correspond to very old SNRs for which electrons have had enough time to lose a significant amount of energy at the highest radio frequencies, and primarily to distant (mainly extragalactic) SNRs for which the limitation in telescope resolution leads to capturing of radio emission from the sample of "exhausted" electrons (Urošević 2014, and references therein). The angular resolution of *Planck's* Low Frequency Instrument (LFI) at 30, 44 and 70 GHz is 33′, 24′, 14′, respectively (Mandolesi et al. 2010). For a comparison, the angular resolution of Wilkinson Microwave Anisotropy Probe (WMAP) at 23, 33, 41, 61 and 94 GHz is around 53′, 40′, 31′, 21′ and 13′, respectively (Bennett et al. 2003). The resolution of WMAP at its lowest frequencies makes it unsuitable for our analysis of the W44 SNR.

In addition, it must be noted that a few examples of concave-down radio spectra of Galactic SNRs can be found in the recent literature, e.g. the cases of SNRs S147 and HB21. Xiao et al. (2008) identified a spectral break at 1.5 GHz for SNR S147 and Pivato et al. (2013) reported steepening at around 6 GHz in the case of SNR HB21. Finally, Planck Collaboration Int. XXXI (2014) reported several other Galactic SNRs with possible high frequency spectral bending (such as IC443 and Puppis A). The high frequency spectral bending starts at relatively lower frequencies (several GHz) for S147 and HB21 than for SNRs W44, IC443 and Puppis A (several tens of GHz).

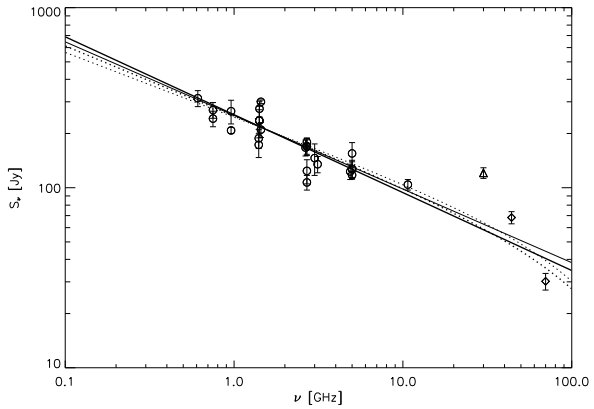

Fig. 1. *The weighted least-squares fit to data for the synchrotron power law model (solid line) as well as for synchrotron power law model with high frequency exponential cut-off (dotted line). Thick and thin lines correspond to the fits without and with inclusion of Planck data at 30 GHz, respectively. Diamond symbols indicate Planck data; the point at 30 GHz is shown as a triangle.*

2.2. The analysis of possible spinning dust emission towards the SNR W44

The spinning dust emission is currently one of the most probable proposed mechanisms to explain the so called anomalous microwave emission[2] (AME) from the diffuse interstellar medium (ISM) of the Milky Way (Planck Collaboration Int. XV 2014,

[2]Dust-correlated emission observed between around $10 - 100$ GHz that can not be accounted for by extrapolating the thermal dust emission to low frequencies.

and references therein). In fact, it is believed that the anomalous component of the diffuse Galactic background is produced by the electric dipole rotational emission from very small dust grains (Erickson 1957, Draine and Lazarian 1998a). Small dust grains are likely to have a nonzero electric dipole moment due to the intrinsic dipole moment of molecules within the grain and uneven charge distribution. These grains will spin due to interaction with the ambient interstellar medium and radiation field, and thus radiate electromagnetic waves due to rotation of their electric dipole moment (Ali-Haïmoud et al. 2009). To calculate the detailed frequency spectrum of spinning dust, one needs to integrate the emission over a distribution of grain sizes, electric dipole moments, and angular velocities (see Dickinson et al. 2014, and references therein for more details). Many recent papers have dealt with additional improvements of the basic emission model (Ali-Haïmoud et al. 2009, Ysard et al. 2010, Ysard and Verstraete 2010, Hoang et al. 2010, 2011, Ysard et al. 2011).

Spinning dust emission can generally significantly contribute at high radio continuum frequencies, especially around 10 - 100 GHz (Draine and Lazarian 1998ab, Ali-Haïmoud et al. 2009, Stevenson 2014, Planck Collaboration Int. XV 2014). It is responsible for a characteristic bump in the high frequency part of the radio continuum.

Scaife et al. (2007) fitted the radio spectrum of Galactic SNR 3C396 with a Warm Neutral Medium (WNM) spinning dust emission model (Draine and Lazarian 1998b), asserting for the first time the possibility of spinning dust (rapidly rotating dust grains) emission from the vicinity of an SNR. Although the claims of possible contribution of thermal bremsstrahlung at high frequencies were addressed by Onić et al. (2012) for SNR 3C396, the same is not applicable in the case of the particular shape of the W44's radio spectrum.

In their study of AME in Galactic clouds, Planck Collaboration Int. XV (2014) listed W48 complex (that contains W44) as one of their candidate regions. However, their conclusions based on a significance level of the AME detection suggest that the excess emission is not statistically significant for this object. On the other hand, they emphasized that many of the so called statistically semi-significant AME regions (those at $2-5\sigma$), such as W48, are likely to be real detections of AME. Planck Collaboration Int. XV (2014) also noted that, in general, the emerging picture is that the bulk of the AME (most probably due to spinning dust) is coming from the polycyclic aromatic hydrocarbons and small dust grains from the colder neutral interstellar medium phase. They also suggested that AME comes from a molecular cloud dust or PDR and not from H II regions themselves. This is consistent with a general belief that PAHs are destroyed in H II regions, and the AME emissivity is lower in the ionized phase of the interstellar medium.

However, Hensley and Draine (2015) voiced their concern on the validity of claims about the AME/PAHs association. They proposed that one possibility is that AME could be in fact a spinning dust emission arising primarily from very small grains that are not PAHs. Of course, the AME could be a combination of the emission from spinning PAHs and non-PAH spinning dust as well as thermal dust emission, such as magnetic dipole emission (Hensley and Draine 2015, and references therein). Hensley and Draine (2015) did not find the evidence for a strong AME correlation with the free-free or CO emission, but they emphasize the plausibility of correlation with synchrotron emission. If the AME arises from spinning ultra small grains, it might be enhanced in SNRs in which grains are violently shattered. In spite of that, it can also be suppressed as the result of the destruction of very small grains by sputtering (Lakićević et al. 2015).

In a recent paper, Irfan et al. (2015) analyzed the region that encompasses SNR W44. The inner aperture size used for their aperture photometry was set to $60'$ and centered around the Galactic coordinates, $l = 34.^{\circ}8$, $b = -0.^{\circ}5$. Irfan et al. (2015) demonstrated the presence of AME associated with that region. They also ruled out the possibility that the excess emission near 30 GHz was from a nearby ultra-compact H II region.

As the proper physical conditions may exist, it is worth checking if the spinning dust emission is significant enough to shape the radio spectrum of W44 SNR near 30 GHz. To that end, the SpDust code, ver. 2.01 (Ali-Haïmoud et al. 2009, Silsbee et al. 2011) was used. The radio continuum spectrum from 610 MHz to 70 GHz was fitted by the sum of synchrotron radiation represented by the power law with spectral index α and the spinning dust emission $S_{\rm spd}(\nu; n, T)$ (Eq. 3):

$$S_{[\rm Jy]}(\nu) = S^{\rm sync}_{[\rm Jy]}(1{\rm GHz})\ \nu^{-\alpha}_{[\rm GHz]} + S_{\rm spd}(\nu; n, T). \quad (3)$$

A spinning dust emission spectrum from a WNM model (assume $n_{\rm H} = 0.4$ cm^{-3}, $T = 6000$ K) was used in fitting the overall radio continuum spectrum as well as several other standard types of environments that were used for comparison: Warm Ionized Medium (WIM, $n_{\rm H} = 0.1$ cm^{-3}, $T = 8000$ K), Cold Neutral Medium (CNM, $n_{\rm H} = 30$ cm^{-3}, $T = 100$ K), and Molecular Cloud (MC, $n_{\rm H} = 300$ cm^{-3}, $T = 20$ K). These idealized ISM phases are defined in Table 1 by Draine and Lazarian (1998b). The parameters for the grain size distribution are taken from Table 1 by Weingartner and Draine (2001) in accordance with Ali-Haïmoud et al. (2009) - see Fig. 14 of their work. Due to the low quality of the radio spectrum we must confine ourselves to a qualitative analysis using standard ISM environments.

The weighted least-squares fit is calculated using the MPFIT[3] (Markwardt 2009) package written in IDL for all of the fits presented in this paper, with starting values estimated from the data. MPFIT

[3]http://purl.com/net/mpfit

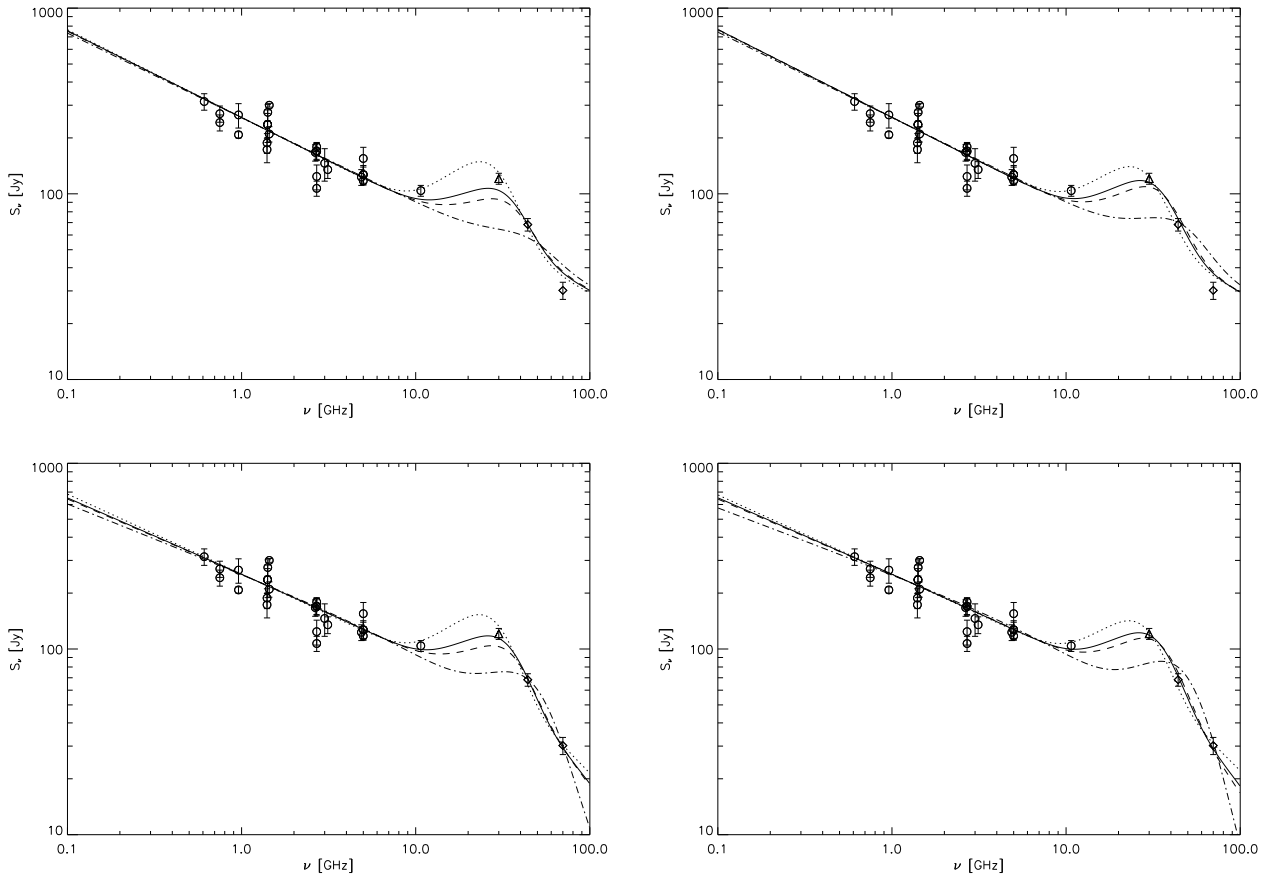

Fig. 2. *The weighted least-squares fit to the data for the synchrotron power law model with inclusion of the spinning dust emission (Eq. 3) is presented in the upper graphs, and the weighted least-squares fit to data for the synchrotron power law model with high frequency exponential cut-off with inclusion of the spinning dust emission (Eq. 4) is presented in the lower graphs. The left and right graphs correspond to the data samples with flux density at 30 GHz excluded and included, respectively. Diamond symbols indicate Planck data and triangle symbol represents the data point at 30 GHz. Different lines correspond to different models of idealized phases of interstellar medium: WIM - solid line, WNM - dotted line, CNM - dashed line, MC - dashed dot line.*

also provides estimates of the 1σ uncertainties for each parameter, taken as the square root of the diagonal elements of the parameter covariance matrix. We must note here that while modeling the spinning dust emission can yield very good fits, one must exercise caution in interpreting these results since the fitted parameters can become unphysical.

Also, it is worth mentioning that in the case of non-linear model fitting, the number of degrees of freedom is generally unknown, i.e. it is not possible to compute the value of reduced χ^2, or the adjusted R^2 (Andrae et al. 2010). In non-linear models, the parameter $k = N - p$ (where N is the number of data points and p is the number of model parameters) does not always represent the exact number of degrees of freedom (Andrae et al. 2010).

The results of weighted least-squares fit to data by Eq. 3 are presented in left and right upper graphs of Fig. 2. The left and right graphs correspond to the data samples with flux density at 30 GHz excluded and included, respectively. Diamond symbols indicate *Planck* data and the triangle symbol represents data at 30 GHz. Different lines correspond to different models of idealized phases of interstellar medium: WIM - solid line, WNM - dotted line, CNM - dashed line, MC - dashed dot line. The best fitting parameters as well as the corresponding χ^2 (k) for different models are presented in Table 1 (star symbol indicates the inclusion of the 30 GHz *Planck* data in the analysis).

The large scatter of flux densities measured at the same frequencies prevents us from making a firm discrimination between the considered models. We cannot rule out the significance of spinning dust emission from this SNR. A model that involves the WNM condition is statistically the most proba-

ble (supported by the standard analysis of χ^2/k values) and also physically plausible for the particular SNR environment. In addition, this model (dotted line in Fig. 2) passes through the error bars of the data point at 30 GHz even when that point is excluded from the analysis. As noted by Planck Collaboration Int. XXXI (2014), this point is possibly contaminated by the unrelated large-scale emission from the Galactic plane. Although such a claim can not be fully dismissed, the strong possibility exists that the spinning dust emission is in fact, at least partially, responsible for the apparent bump around 30 GHz.

For completeness, the spinning dust flux density estimate $S_{\rm spd}(30)$, as well as its ratio to the total flux density $f(30) = S_{\rm spd}(30)/S(30)$ at 30 GHz is given in Table 1 for all considered models. The spinning dust fractions $f(30)$ are in accordance with the results obtained for other AME sources (≈ 0.5) in Planck Collaboration Int. XV (2014).

Additional support for a spinning dust emission hypothesis can be found in its correlation with thermal dust emission, especially at IRAS (Infrared Astronomical Satellite) wavelengths. Planck Collaboration Int. XV (2014) found that AME sources generally have a 12 μm/25 μm ratio $\approx (0.6 - 1.0)$. This is interpreted as a confirmation of the spinning dust model where the very small grains are responsible for the bulk of the AME. Although the W44 SNR was not detected by Saken et al. (1992), Arendt (1989) found a 12 μm/25 μm ratio of ≈ 1. However, the possibility of ionic line contamination of the particular IRAS bands can not be fully dismissed (Oliva et al. 1999, Reach and Rho 1996).

The comparison was also made between the spinning dust flux density estimates at 30 GHz $S_{\rm spd}(30)$ for different models to the 100 μm (3000 GHz) flux density $S(3000)$ as given in Arendt (1989). The ratio $S_{\rm spd}(30)/S(3000)$ spans a large range of values for the different environmental models: $(7 - 60) \times 10^{-4}$. Bearing in mind the roughness of our analysis, as well as high uncertainty of the IRAS 100 μm flux density (around 50%), our values for $S_{\rm spd}(30)/S(3000)$ are in a rough agreement (slightly higher) with other determinations for AME sources ($(1-15)\times 10^{-4}$, Planck Collaboration Int. XV 2014, Hensley and Draine 2015, and references therein).

Finally, it is tempting to check whether the fits will improve if the model that incorporates the sum of power law with exponential cut-off and the spinning dust emission is used (Eq. 4):

Table 1. The best fitting parameters for different models.

Equation	α	ν_0 [GHz]	$S_{\rm spd}(30)$ [Jy]	$f(30)$	χ^2 (k)
1	0.433 ± 0.014	–	–	–	268.18 (26)
1*	0.409 ± 0.013	–	–	–	322.11 (27)
2	0.388 ± 0.024	234 ± 109	–	–	262.84 (25)
2*	0.358 ± 0.023	220 ± 91	–	–	315.13 (26)
3 (WIM)	0.467 ± 0.018	–	51.6 ± 12.9	0.50 ± 0.20	251.76 (25)
3*(WIM)	0.473 ± 0.017	–	63.5 ± 7.7	0.55 ± 0.12	253.13 (26)
3 (WNM)	0.473 ± 0.018	–	78.7 ± 18.0	0.60 ± 0.24	248.63 (25)
3*(WNM)	0.470 ± 0.017	–	70.6 ± 8.3	0.57 ± 0.12	248.90 (26)
3 (CNM)	0.465 ± 0.018	–	40.1 ± 10.6	0.43 ± 0.18	253.60 (25)
3*(CNM)	0.473 ± 0.017	–	57.1 ± 7.2	0.52 ± 0.12	258.53 (26)
3 (MC)	0.456 ± 0.019	–	9.7 ± 5.0	0.15 ± 0.10	264.09 (25)
3*(MC)	0.460 ± 0.019	–	20.3 ± 4.7	0.27 ± 0.10	303.06 (26)
4 (WIM)	0.408 ± 0.025	136 ± 46	63.2 ± 13.7	0.55 ± 0.23	241.14 (24)
4*(WIM)	0.409 ± 0.025	130 ± 42	68.4 ± 8.0	0.58 ± 0.15	241.35 (25)
4 (WNM)	0.428 ± 0.027	196 ± 88	81.7 ± 18.3	0.62 ± 0.26	242.93 (24)
4*(WNM)	0.424 ± 0.026	203 ± 91	71.3 ± 8.4	0.58 ± 0.15	243.34 (25)
4 (CNM)	0.403 ± 0.025	127 ± 42	52.0 ± 11.5	0.51 ± 0.21	241.83 (24)
4*(CNM)	0.402 ± 0.025	112 ± 33	64.0 ± 7.7	0.56 ± 0.15	243.75 (25)
4 (MC)	0.374 ± 0.028	61 ± 22	31.5 ± 7.9	0.42 ± 0.22	243.32 (24)
4*(MC)	0.354 ± 0.031	47 ± 17	43.4 ± 8.1	0.52 ± 0.23	268.05 (25)

*Analysis includes 30 GHz Planck data.

$$S_{[\mathrm{Jy}]}(\nu) = S^{\mathrm{sync}}_{[\mathrm{Jy}]}(1\mathrm{GHz})\ \nu^{-\alpha}_{[\mathrm{GHz}]}\ e^{-\frac{\nu}{\nu_0}} + S_{\mathrm{spd}}(\nu; n, T). \quad (4)$$

The lower graphs of Fig. 2 represent the weighted least-squares fit to the data for the synchrotron power law model with high frequency exponential cut-off with inclusion of spinning dust emission (Eq. 4). The left and right graphs correspond to the data samples with flux density at 30 GHz excluded and included, respectively. The best fitting parameters as well as the corresponding χ^2 (k) for different models are given in Table 1.

The average χ^2/k is slightly less for Eq. 4 than for Eq. 3 (see Table 1). On the other hand, statistical discrimination between different environmental conditions used for Eq. 4, is in this case, even more inconclusive. Yet the detection of hard X-ray emission from W44, not connected with associated pulsar or its nebula reported by Uchida et al. (2012), can cast doubt that the high frequency synchrotron cut-off at around 100 - 200 GHz (see Table 1) is genuine and is primarily responsible for a lower flux density at 70 GHz. On the other hand, Lee et al. (2015) recently explored the non-thermal emission mechanisms of dynamically evolved SNRs. They explored two scenarios of particle acceleration: either a re-acceleration of Galactic cosmic rays, or an efficient nonlinear diffusive shock acceleration of thermally injected particles by a fast radiative cloud shock. Lee et al. (2015) emphasized that if a sufficiently strong magnetic turbulence is present in the molecular cloud, the re-acceleration scenario of the non-thermal emission agrees well with the broadband spectrum of SNR W44 and the apparent discrepancy at 30 GHz can possibly arise from the anomalous microwave emission from small spinning dust grains. Their predicted radio spectrum shows a spectral softening above around 10 GHz due to synchrotron loss, and is consistent with the 70 GHz flux density from *Planck*.

One must bear in mind that the SNR W44 is actually located in a very complex region. The physical conditions inside the remnant may vary significantly. A more detailed radiative transfer model than the one presented in this paper should be considered to further our understanding of the spinning dust emission and its significance. Finally, the statistically insufficient number of flux density samples prevents us from making a firm quantitative discrimination between different models. In addition to the general need for more data, the much more improved resolution ($< 1'$) of new observations at radio continuum frequencies between 10 and 100 GHz would also be beneficial.

3. CONCLUSIONS

In this paper, the integrated radio spectrum of SNR W44 was analyzed up to 70 GHz through testing different emission models that can be responsible for its particular shape. The main conclusions are:

(1) *Planck* observations made it possible to analyze the high frequency part of radio emission from SNRs.
(2) Although the quality of radio continuum spectrum (a high scatter of data points at same frequencies) prevents us from making definite conclusions, the possibility of spinning dust emission detection towards this remnant is emphasized. In fact, the spinning dust emission is proposed to be, at least partially, responsible for the apparent bump in the radio continuum around 30 GHz.
(3) In addition the concave-down feature in the radio spectrum, due to synchrotron losses, can not be definitely dismissed by the present knowledge of the radio continuum spectrum of this SNR.
(4) Finally, more data at different frequencies between 10 and 100 GHz at much better resolution than *Planck* are needed to make firm conclusions about the contribution of particular radiation mechanisms responsible for an observed shape of the radio spectrum of SNR W44.

Acknowledgements – I want to thank Dejan Urošević for careful reading of the manuscript and useful comments that substantially improved this paper. I am also grateful to T. Hoang as well as to the anonymous referee for valuable suggestions. This work is part of Project No. 176005 "Emission Nebulae: Structure and Evolution" supported by the Ministry of Education, Science, and Technological Development of the Republic of Serbia.

REFERENCES

Ali-Haïmoud, Y., Hirata, C. and Dickinson, C.: 2009, *Mon. Not. R. Astron. Soc.*, **395**, 1055.
Altenhoff, W. J., Downes, D., Goad, L., Maxwell, A. and Rinehart, R.: 1970, *Astron. Astrophys*, **1**, 319.
Anderl, S., Gusdorf, A. and Güsten, R.: 2014, *Astron. Astrophys*, **569**, 81.
Andrae, R., Schulze-Hartung, T. and Melchior, P.: 2010, arXiv:1012.3754.
Arendt, R. G.: 1989, *Astrohys. J. Suppl. S.*, **70**, 181.
Baars, J. W. M, Genzel, R., Pauliny-Toth, I. I. K. and Witzel, A.: 1977, *Astron. Astrophys*, **61**, 99.
Bennett, C. L. et al.: 2003, *Astrophys. J.*, **583**, 1.
Cardillo, M., Tavani, M., Giuliani, A., Yoshiike, S., Sano, H., Fukuda, T., Fukui, Y., Castelletti, G. and Dubner, G.: 2014, *Astron. Astrophys*, **565**, 3754.
Castelletti, G., Dubner, G., Brogan, C. and Kassim, N.E.: 2007, *Astron. Astrophys*, **471**, 537.
Dickinson, C. Ali-Haïmoud, Y., Beswick, R. J., Casassus, S., Cleary, K., Draine, B. T., Genova-Santos, R., Grainge, K., Hoang, T. C., Lazarian, A. et al.: 2014, arXiv:1412.5054.
Draine, B. T. and Lazarian A.: 1998a, *Astrophys. J. Lett.*, **494**, L19.

Draine, B. T. and Lazarian A.: 1998b, *Astrophys. J.*, **508**, 157.
Erickson, W. C.: 1957, *Astrophys. J.*, **126**, 480.
Green D. A., 2014, 'A Catalogue of Galactic Supernova Remnants (2014 May version)', Cavendish Laboratory, Cambridge, United Kingdom (available at "http://www.mrao.cam.ac.uk/surveys/snrs/").
Hensley, B. S. and Draine, B. T.: 2015, arXiv:1505.02157.
Hoang, T., Draine, B. T. and Lazarian, A.: 2010, *Astrophys. J.*, **715**, 1462.
Hoang, T., Lazarian, A. and Draine, B. T.: 2011, *Astrophys. J.*, **741**, 87.
Irfan, M. O., Dickinson, C., Davies, R. D. et al.: 2015, *Mon. Not. R. Astron. Soc.*, **448**, 3572.
Lakićević, M., van Loon, J. T., Meixner, M. et al.: 2015, *Astrophys. J.*, **799**, 50.
Lee, S-H., Patnaude, D. J., Raymond, J. C., Nagataki, S., Slane, P. O. and Ellison, D. C.: 2015, *Astrophys. J.*, **806**, 71
Mandolesi, N., Bersanelli, M., Butler, R. C. et al.: 2010, *Astron. Astrophys*, **520**, 3.
Markwardt, C. B.: 2009, ASP. Conf. Ser., **411**, 251.
Oliva, E., Lutz, D., Drapatz, S. and Moorwood, A. F. M., 1999, *Astron. Astrophys*, **341**, 75.
Onić, D.: 2013, *Astrophys. Space Sci.*, **346**, 3.
Onić, D., Urošević, D., Arbutina, B. and Leahy, D.: 2012, *Astrophys. J.*, **756**, 61.
Ortega, M. E., Paron, S., Cichowolski, S., Rubio, M., Castelletti, G. and Dubner, G.: 2010, *Astron. Astrophys*, **510**, 96.
Paron, S., Ortega, M. E., Rubio, M. and Dubner, G.: 2009, *Astron. Astrophys*, **498**, 445.
Pivato, G., Hewitt, J. W., Tibaldo, L., Acero, F., Ballet, J., Brandt, T. J., de Palma, F., Giordano, F., Janssen, G. H., Jóhannesson, G. and Smith, D. A.: 2013, *Astrophys. J.*, **779**, 179.
Planck Collaboration Int. XV: Ade, P. A. R., Aghanim, N., Alves, M. I. R. et al.: 2014, *Astron. Astrophys*, **565**, 103.
Planck Collaboration Int. XXXI: Arnaud, M., Ashdown, M., Atrio-Barandela, F. et al.: 2014, arXiv:1409.5746.
Reach, W. T. and Rho, J.: 1996, *Astron. Astrophys*, **315**, 277.
Rho, J. and Petre, R.: 1998, *Astrophys. J.*, **503**, L167.
Saken, J. M., Fesen, R. A. and Shull, J. M.: 1992, *Astrohys. J. Suppl. S.*, **81**, 715.
Scaife, A., Green, D. A., Battye, R. A. et al.: 2007, *Mon. Not. R. Astron. Soc.*, **377**, L69.
Silsbee, K., Ali-Haïmoud, Y. and Hirata C.: 2011, *Mon. Not. R. Astron. Soc.*, **411**, 2750.
Stevenson, M. A.: 2014, *Astrophys. J.*, **781**, 113.
Sun, X. H., Reich, P., Reich, W., Xiao, L., Gao, X. Y. and Han, J. L.: 2011, *Astron. Astrophys*, **536**, 83.
Uchida, H., Koyama, K., Yamaguchi, H., Sawada, M., Ohnishi, T., Tsuru, T., Go., Tanaka, T., Yoshiike, S. and Fukui, Y.: 2012, *Publ. Astron. Soc Jpn.*, **64**, 141.
Urošević, D.: 2014, *Astrophys. Space Sci.*, **354**, 541.
Vink, J.: 2012, *Astron. Astrophys. Rev.*, **20**, 49.
Weingartner J. C. and Draine B. T.: 2001, *Astrophys. J.*, **548**, 296.
Xiao, L., Fürst, E., Reich, W. and Han, J. L., 2008, *Astron. Astrophys*, **482**, 783.
Ysard, N., Miville-Deschênes, M. A. and Verstraete, L.: 2010, *Astron. Astrophys*, **509**, 1.
Ysard, N. and Verstraete, L.: 2010, *Astron. Astrophys*, **509**, 12.
Ysard, N., Juvela, M. and Verstraete, L.: 2011, *Astron. Astrophys*, **535**, 89.
Yoshiike, S., Fukuda, T., Sano, H., Ohama, A., Moribe, N., Torii, K., Hayakawa, T., Okuda, T., Yamamoto, H., Tajima, H. et al.: 2013, *Astrophys. J.*, **768**, 179.

О ИНТЕГРАЛНОМ НЕПРЕКИДНОМ РАДИО-СПЕКТРУ ОСТАТКА СУПЕРНОВЕ W44 (G34.7-0.4): НОВА САЗНАЊА ПОМОЋУ ПЛАНКА

D. Onić

Department of Astronomy, Faculty of Mathematics, University of Belgrade
Studentski trg 16, 11000 Belgrade, Serbia

E–mail: *donic@math.rs*

УДК 524.354–77
Оригинални научни рад

У овом раду је анализиран интегрални непрекидни радио-спектар остатка супернове (ОСН) W44 све до 70 GHz и тестирани су различити емисиони модели који могу узроковати његов својеврсни облик. Посматрања реализована свемирским телескопом Планк омогућила су да се анализира високофреквентни део радио-емисије ОСН. Иако је квалитет непрекидног радио-спектра (велико расипање вредности на истим фреквенцијама) такав да нам онемогућава да изведемо чврсте закључке, истакнута је највероватнија детекција емисије ротирајуће прашине у правцу овог остатка. Уз то, тренутно познавање интегралног непрекидног радио-спектра овог ОСН није довољно да би се дефинитивно могла оспорити тврдња о конкавном кривљењу спектра услед синхротронских губитака.